Configurational evidence for antiferromagnetic interaction in disordered magnetic ionic liquids by X-ray scattering-aided hybrid reverse Monte Carlo simulation

Ryusuke Futamura[1]*, Yuma Takasaki[1], Hayato Otsuka[1,2], Sumio Ozeki[1], Katsumi Kaneko[2] and Taku Iiyama[1,2]*

[1]*Faculty of Science, Department of Chemistry, Shinshu University, 3-1-1, Asahi, Matsumoto-City, 390-8621, Japan*

[2] *Research Initiative for Supra-Materials, Shinshu University, 4-17-1, Wakasato, Nagano-City, 380-8553, Japan*

* E-mail: ryu_f@shinshu-u.ac.jp; tiiyama@shinshu-uac.jp

Abstract

Magnetic ionic liquids (MIL) are a new type of ionic liquids that show paramagnetic response to magnetic fields. Here, we elucidate a plausible 3D liquid structure of the 1-ethyl-3-methyl-imidazolium tetrachloroferate (Emim[$FeCl_4$]) and 1-butyl-3-methyl-imidazolium tetrachloroferate (Bmim[$FeCl_4$]) MILs by X-ray scattering-aided hybrid reverse Monte Carlo simulations. Bmim[$FeCl_4$] showed anomalously continuous structural changes over a wide temperature range (90–523 K) without crystallization, while Emim[$FeCl_4$] displayed a melting point at 291 K with no glass transition.

Conventional electron radial distribution function (ERDF) analysis provides misleading information about the structures of these MILs due to the mutual cancellation of the partial anion-anion and anion-cation ERDFs. Subsequent hybrid reverse Monte Carlo (HRMC) analysis revealed the precise coordination structures of both ionic liquids, and the alternating periodic arrangement of the anions and cations was visualized based on

the HRMC simulation results. The results clearly revealed that the 1st coordination structure of the $FeCl_4$ anion around the Bmim cation was widespread compared to that of the Emim cation, resulting in the absence of crystallization. In addition, we obtained new insights into the antiferromagnetic interaction between the $FeCl_4^-$ ions of Bmim[$FeCl_4$] even in the absence of the crystallization at low temperatures. Our results shed new light on the development of MILs not only for practical applications but also for the advancing the basic science of pure liquids with a high magnetic response.

Key words

Magnetic Ionic liquids, X-ray scattering, Hybrid reverse Monte Carlo simulation, Coordination structure, Antiferromagnetic interaction, Amorphous structure

1. Introduction

Room-temperature molten salts that are well known as ionic liquids (ILs) have many unique properties such as negligible vapor pressure and high electric conductivity [1-3]. ILs are also called designer solvents because their compositions and desired properties can be theoretically chosen and synthesized from millions of possible compositions [4]. In 2004, Hamaguchi et al. determined a new type of IL, 1-butyl-3-methyl-imidazolium tetrachloroferate (Bmim[$FeCl_4$]), that exhibits paramagnetism because it contains an inorganic cation of the Fe(III) transition metal even in a pure liquid state at room

temperature, thereby reporting the so-called magnetic ionic liquids (MILs) [5]. Following this work, research on MILs has mainly focused on the synthesis of new MILs and the determination of their magnetic properties [6-9] because of their important applications [10,11] and fundamental interests in the high magnetic response of liquids [5,12]. Moreover, another MIL, namely, 1-ethyl-3-methyl-imidazolium tetrachloroferate (Emim[$FeCl_4$]), has attracted attention because of the Néel transition in which the MILs undergo a change from paramagnetic to antiferromagnetic behavior at 3.8 K [13-15]. It is necessary to understand the magnetism and the magnetic phase transition of MILs for the elucidation of the intermolecular structures of ILs that are controlled not only by the superexchange interaction between the magnetic moments of magnetic ions [7] but also by Coulombic ordering and domain structure formation due to the unique intermolecular interactions between the ions (i.e., Coulombic interaction, hydrogen bonds, and van der Waals interactions) [16].

In addition, organic-inorganic hybrid functional materials have recently attracted much attention as potential agents in extremely diverse applications because of their outstanding chemical and physical properties derived from the synergetic effects of their organic and inorganic moieties [17,18]. MILs can also be regarded as hybrid materials that are composed of a charge-delocalized bulky organic cation and an inorganic anion of

a transition metal ligand with a magnetic moment. Among the wide variety of organic-inorganic hybrid functional materials, the MILs show the unique feature of a liquid state with both ionic conductivity and magnetic response at room temperature.

However, although the MIL crystal structures at low temperatures have been extensively investigated, the liquid structures of MILs have still not been elucidated because of the difficulties involved in their analysis [7,12-15]. Conventionally, structural analyses of molecular liquids [19], aqueous solutions [20], and simple ILs such as 1-butyl-3-methyl-imidazolium iodide (BmimI) [21] have been conducted using electron radial distribution functions (ERDFs) that are obtained by the Fourier transformation of X-ray scattering profiles. However, as shown here, it is difficult to use these methods to understand multicomponent systems such as ILs. Other methods for understanding liquid structures are based on molecular simulations [22] or methods combining molecular simulations and experimental techniques such as X-ray scattering and NMR measurements [20,23-25]; however, these methods have not been applied to the MIL systems.

Recently, we applied an experimental-derived molecular simulation method of hybrid reverse Monte Carlo (HRMC) simulation to determine the molecular structure that was in good agreement with the X-ray scattering profiles of IL systems [26]. In the present work, using this method, we studied the structure of the MILs at a range of temperatures

from room temperature to low temperatures. Our results provide new insight into the antiferromagnetic interaction between the $FeCl_4^-$ ions of Bmim[$FeCl_4$] found even in the absence of the transition to the crystal phase at low temperature.

2. Experimental

2.1. X-ray scattering measurements

Emim[$FeCl_4$] (>98 wt%, Tokyo Chemical Industry Co., Ltd.) and Bmim[$FeCl_4$] (> 98 wt%, Tokyo Chemical Industry Co., Ltd.) MILs were used without further purification. X-ray scattering measurements of the MILs in glass capillaries with the diameter and thickness of 0.7 mm and 0.01 mm, respectively, were carried out in the synchrotron radiation facility of SPring-8 with an imaging plate (IP) as the detector. The wavelength (λ = 0.07997 nm) monochromated with a Si (111) plane was determined using CeO_2 powder (cubic crystal system with a lattice parameter of 0.54111 nm). The X-ray scattering profile of a glass capillary without samples was also measured for background correction. These measurements were conducted for 20 min for each sample. The temperature dependence of the X-ray scattering profiles of both MILs was also measured in the temperature range of 90-523 K. The temperature was controlled using cooled or heated nitrogen gas flow.

2.2. HRMC simulation

We determined the plausible intermolecular structures of Emim[$FeCl_4$] and Bmim[$FeCl_4$] that reproduced the experimental X-ray scattering profile with high accuracy using a molecular simulation protocol based on the reverse Monte Carlo (RMC) method in which both the total energy of the system and the sum of the residual between the experimental and simulated structure factors are minimized; this is known as hybrid reverse Monte Carlo (HRMC) simulations [27,28]. The details of the simulation method can be found in previous reports [26-28]. Briefly, acceptance probability P_{acc} in the conventional MC simulation is modified in our HRMC method as follows:

$$P_{\mathrm{acc}} = \min[1, \exp\left(-\frac{\chi^2_{\mathrm{new}} - \chi^2_{\mathrm{old}}}{w_{\mathrm{X}}}\right) \times \exp\left(\frac{E_{\mathrm{new}} - E_{\mathrm{old}}}{k_{\mathrm{B}}T}\right)]$$

where χ^2 is the residual sum of squares between the experimental (S_{exp}) and simulated (S_{sim}) X-ray scattering structural factors, $\chi^2 = \sum_{i=0}^{n}(S_{\mathrm{exp}}(s_i) - S_{\mathrm{sim}}(s_i))^2$, E is the potential energy of the system, w_x is the weighting parameter, T is the temperature, and k_B is the Boltzmann constant. The subscripts "new" and "old" mean after and before the trial, respectively. Lennard-Jones and Coulombic interactions were considered for the intermolecular interaction terms. The molecular structure, LJ parameters, and Coulombic parameters of the ions are listed in the Supplemental Information (SI). The geometry and point charges of the $FeCl_4^-$ and Bmim ions were determined based on density functional theory (DFT) calculations carried out using the Gaussian 09 package [29]. DFT

calculations were performed using the hybrid B3LYP exchange-correlation functional with the LANL2DZ basis set for Fe (III) and the 6-311+G(2d,2p) basis set for the other elements. All optimized configurations were confirmed to be potential energy minima by vibrational frequency calculations. Finally, the most stable configurations of the ions were used for the subsequent atomic point charge calculations carried out using the charges from electrostatic potential grid (CHelpG) method [30,31].

In HRMC simulations, a rigid model was employed for the molecular structure of the nonplanar staggered model of the Emim ions [25] and the *TT* butyl chain model of the Bmim ions [32]. The simulated temperatures, *T*, were set to the experimental temperatures, that is, T = 298.15 K for the Emim[$FeCl_4$] system, and T = 90.15, 298.15, and 523.15 K for Bmim[$FeCl_4$]. The temperatures were fixed throughout the simulations for all runs. The number of ion pairs, *N*, was 610 for Emim[$FeCl_4$], while for Bmim[$FeCl_4$], *N* was 526 at 90.15 and 298.15 K and was 472 at 527 K. The *N* pairs of cations and anions were placed in the cubic simulation box ($6 \times 6 \times 6$ nm^3) at random, and then HRMC simulations were started in the *NVT* ensemble. HRMC simulations were conducted until the potential energy equilibrium of the systems was attained (i.e., at least for 2×10^7 steps), and the configurational information for the final 1×10^6 steps of the HRMC simulations was used. Further details of the HRMC simulations are described in

SI.

3. Results and Discussions

Figure 1 shows the corrected X-ray scattering profiles of Emim[$FeCl_4$] (black) and Bmim[$FeCl_4$] (red) at room temperature. The correction method for the X-ray scattering profiles is described in the SI and in our previous reports [26,33]. For both profiles, three peaks are observed at $s < 20$ nm^{-1}, at s = 9.4, 12.5, and 18.2 nm^{-1} for Bmim[$FeCl_4$] and at s = 9.0, 12.7, and 18.3 nm^{-1} for Emim[$FeCl_4$], that are attributed to the intermolecular periodicities of these MILs. Here, s ($= 4\pi\sin\theta/\lambda = 2\pi/d$) is the scattering parameter. While the profiles of the two MILs are similar, the relative intensities of the three peaks are different, as are the peak positions; the 1st and 3rd peak intensities (d = 0.70 and 0.34 nm, respectively) are relatively small, but the 2nd peak intensity (d = 0.49 nm) is relatively high for Bmim[$FeCl_4$] compared to those for Emim[$FeCl_4$]. The differences between these profiles provide detailed information about the coordination structures of both MILs as will be discussed below based on the results of HRMC simulation.

Figures 2(a) and (b) show the ERDFs of Emim[$FeCl_4$] and Bmim[$FeCl_4$] obtained by the Fourier transform of structure function $S_{exp}(s)$ as open circles. The method used for the derivation of ERDFs was described in our previous works [26,33]. The peaks located

at 0.22 and 0.38 nm are attributed to the intramolecular distances of the $FeCl_4^-$ ions, namely, the distance of the Fe–Cl bond (0.22 nm) and the distance between two Cl atoms that are not bonded to each other (0.38 nm). The peak intensity of Emim[$FeCl_4$] at 0.7 nm that corresponds to the 3rd peak of the X-ray scattering profiles with d = 0.70 nm is higher than that for Bmim[$FeCl_4$]. The ERDFs obtained with HRMC simulation are also shown with solid lines in the same figures. It is observed that the simulated ERDFs show fairly good correspondence to the experimental data, indicating that we can obtain plausible structures of MILs from HRMC simulations. The different contributions for the simulated ERDFs of Emim[$FeCl_4$] and Bmim[$FeCl_4$] (i.e., intra-molecular structure (sky blue) and cation-cation (red), anion-anion (green), and cation-anion (blue) components) are shown in Figures 2(c) and (d), respectively. Both MILs have structures with Coulombic ordering structures with alternating arrays of anions and cations, as reported for other ILs [16,25]. Interestingly, the first coordination peak between cations and anions located at 0.5 nm that corresponds to the 2nd peak of the X-ray scattering profiles with d = 0.49 nm cannot be clearly observed in a broad valley in the experimental ERDFs. This is due to the mutual cancelation by the curves of the cation-anion and anion-anion contributions in the summation that arises from their comparable but opposite sign of amplitudes of the component ERDFs. This indicates that it is difficult to obtain detailed structural

understanding in these systems using the conventional ERDF methods only. The higher intensity for the cation-anion ERDF at 0.5 nm for Bmim[$FeCl_4$] implies a larger coordination site of the $FeCl_4^-$ ion around the Bmim ions compared to that around the Emim ions, as discussed below. On the other hand, the higher intensity for ERDFs in the 0.6-0.9 nm range for Emim[$FeCl_4$] in Figure 2(a) can be attributed to the shift of 1st peak position for the anion-anion ERDFs (green) in Figure 2(c) to a lower position compared to that of Bmim[$FeCl_4$] in Figure 2(d) (i.e. 0.89 nm for Emim[$FeCl_4$] and 0.96 nm for Bmim[$FeCl_4$]). The anion-anion intermolecular structure is very important for understanding the magnetism of MILs [7], particularly at low temperatures, as discussed below.

The 1st coordination structures around the Emim and Bmim cations were analyzed using spatial distribution functions (SDFs) [25]. Figure 3 shows the SDFs of the Fe atoms of $FeCl_4^-$ around the N1 atoms of the Emim and Bmim cations that have a chemical bond with an ethyl or a butyl group. For Emim[$FeCl_4$] (Figs. 3(a)-(c)), the $FeCl_4^-$ ion coordinates 4 distinct sites around the Emim ions: the upward (A) and downward (B) imidazolium ring planes and both sides of the ethyl chain (C, D). For Bmim[$FeCl_4$] (Figs. 3(d)–(f)), the other site (i.e., the side of methyl chain (E)) is also observed in addition to a similar distribution for Emim[$FeCl_4$]. Furthermore, the two sites (A) and (C) are not

separated from each other for Bmim[$FeCl_4$], indicating the widespread coordination structure of $FeCl_4^-$ particularly around the imidazolium ring. This is related to the non-crystallization behavior of Bmim[$FeCl_4$] at low temperatures.

The crystal structure of Emim[$FeCl_4$] at low temperature has been investigated using XRD measurements due to the interests for the antiferromagnetic properties reported in several studies [14,15]. The melting temperature of Emim[$FeCl_4$] was 291 K, and no glass transition was observed [34]. On the other hand, low-temperature structure analysis for Bmim[$FeCl_4$] is still insufficient. Yoshida et al. reported the glass transition at 185 K and the absence of crystallization by cooling and the subsequent heating process by differential scanning calorimetry measurements [34]. Their experimental results are related to the difficulties in the formation of the crystal structure by the bulky Bmim cation due to the presence of several conformers [32] in addition to the widespread coordination structure, as shown above. Here, we measured the temperature dependence of the X-ray scattering profiles of Bmim[$FeCl_4$] in the temperature range from 90 K to 523 K (Figure 4(a)). The X-ray scattering profile of Bmim[$FeCl_4$] maintained a liquid-type shape with gently decreasing curves with broad peaks even at 90 K, indicating the amorphous solid (glass) structure of Bmim[$FeCl_4$] at 90 K. The profiles gradually change over a wide temperature range from 90 K to 523 K: the peak positions at 9, 13, and 19

nm^{-1} decrease and the peak intensities at 9 and 13 nm^{-1} increase, whereas the peak intensity at 19 nm^{-1} decreases as the temperature increases. On the other hand, the X-ray scattering profile of Emim[$FeCl_4$] at 90 K is a typical crystal diffraction pattern (see Fig. S2). The ERDFs of Bmim[$FeCl_4$] at 90, 298, and 523 K are shown in Figure 4(b). The peak intensities at 0.38, 0.71, and 1.0 nm decreased and the peak position at 1.5 nm increased with increasing temperature. The HRMC simulation elucidates the structural change of Bmim[$FeCl_4$] at the cryogenic (90 K) and high (523 K) temperatures. The temperature dependence of the SDFs of Bmim[$FeCl_4$] in the 1st coordination structure of Fe around the Bmim ion is shown in Figure 5. A gradual decrease in the high distribution region of the $FeCl_4^-$ ions was observed as the temperature increased. Furthermore, the coordination sites became more widespread at low temperature, that is, the A, B, and C sites are connected to each other at 90 K. It is interesting that the delocalization of the coordination structure of counter ions around Bmim ion is opposite tendency from the aspect of low molecular motion at low temperature. These SDF changes indicate the lack of the crystallization for Bmim[$FeCl_4$].

Finally, the temperature dependence of the $FeCl_4^-$-$FeCl_4^-$ ERDFs is shown in Figure 4(c). It is observed that a new peak and a new shoulder appeared at 0.36 nm and 0.75 nm in the profile obtained at 90 K, respectively. In particular, the intensity increase at 0.38 nm

in the experimental ERDF at 90 K (i.e., the red curve in Fig. 4 (b)) could also be attributed to the appearance of the new peak of 0.36 nm in the $FeCl_4^-$-$FeCl_4^-$ ERDF as well as to the population increase in the 1st coordination shell of $FeCl_4^-$ ions around the Bmim ions at the low temperature (see Fig. 5). The new peak can be assigned to the Cl · · · Cl interatomic distances between the neighboring $FeCl_4^-$ ions, indicating a clear intermolecular ordering between the anions at low temperatures (see Fig. S3). Despite the absence of a long-range ordered structure between the anions of Bmim[$FeCl_4$] even at 90 K, the glass state is frozen with regard to the transitional and rotational motions of these molecules, giving rise to the certain special coordination positions between the neighboring anions[35]. The inset in Fig. 4(c) shows the SDFs of the neighboring Cl atoms of the $FeCl_4^-$ ions around a central $FeCl_4^-$ ion with a Cl · · · Cl distance within 0.39 nm. This indicates that the nearest neighbor Cl atoms are located not on the extended straight lines of the Fe-Cl bonds (J_1 pathway, see below) but rather on the groove triangular sites composed of the 3 Cl atoms of a $FeCl_4^-$ ion (either J_2 or J_3 pathways, see below). This may be related to the superexchange interaction of the $FeCl_4^-$ ions and the antiferromagnetic interaction between the magnetic moments of $FeCl_4^-$ that give rise to the negative Weiss temperature of MILs [11,12,34,36] and can be explained well by our results. In particular, the clear interaction between the $FeCl_4^-$ ions at the low temperature is revealed for the first time

with our HRMC simulation because Bmim[$FeCl_4$] is found in a glass state at low temperatures without distinct structural features.

It is important to compare the amorphous structure of Bmim[$FeCl_4$] to the crystal structures of similar MILs. García-Saiz et al. demonstrated the plausible exchange pathway of the superexchange interaction of 1,3-dimethylididazolium tetrafluoroferrate (III) (Dimim[$FeCl_4$]) using neutron diffraction measurements at 9 K [7]. They found that Dimim[$FeCl_4$] forms a non-centrosymmetric orthorhombic structure in the $P2_12_12_1$ space group at 9 K. The anion planes and cation planes that are parallel to the *ac* plane stack alternatingly along the *b* axis (see Fig. S4). There are 3 possible pathways for the superexchange interaction of Dimim[$FeCl_4$] at low temperatures: the first for the interplane interaction of the zig-zag chains propagating along the *b* direction with two Fe-Cl-Cl-Fe connections denoted as $J_\perp$ or J_1 (red line in Fig. S5) and the other two for the intraplane interactions that connect the iron atoms in the zig-zag chains in the *ac* plane denoted as $J_\parallel$ (J_2 and J_3, blue and black lines in Fig S5). Here, the non-bonded Cl-Cl distances are 0.3871 nm for the J_1 pathway, 0.3808 nm for the J_2 pathway, and 0.3631 nm for the J_3 pathway. Although $J_\perp$ is a stronger interaction than $J_\parallel$ due to the antiferromagnetic coupling for the Fe-Cl-Cl angles of nearly 180 ° for $J_\perp$ in the crystal structure of Dimim[$FeCl_4$], both interactions are antiferromagnetic and have negative

values (i.e., $J_{\perp}$ = -0.511 K and $J_{\parallel}$ = -0.329 K). For our present results, the nearest neighbor of the Cl atom is located at the groove triangular sites composed of the 3 Cl atoms of a $FeCl_4^-$ ion, and has a similar coordination not to the interplane structure (i.e., the J_1 pathway) but to the intraplane structure (i.e., J_2 or J_3 pathway) even in the amorphous state of Bmim[$FeCl_4$]. This implies that there are magnetic exchange pathways between the $FeCl_4^-$ ions at least for the nearest neighbors, even though the network of the antiferromagnetic interaction does not extend 3-dimensionally in the amorphous structure. Figure 6 shows the distribution of the assembling number of neighboring $FeCl_4^-$ ions in Bmim[$FeCl_4$] at 90 K obtained from the HRMC results. Here, we defined the Cl-Cl neighbor distance as less than 0.39 nm. Although 40% of the $FeCl_4^-$ ions were isolated, more than 50% were assembled into networks. In addition, 35% of the assemblies were composed of more than 3 $FeCl_4^-$ ions. The inset shows selected 3-, 4-, 5-, and 6-member networks of the $FeCl_4^-$ ions. The red lines connect the Fe atoms to the Fe-Cl-Cl-Fe networks. It is evident that the networks are composed of zig-zag pathways that are related to the antiferromagnetic interactions of Bmim[$FeCl_4$] at low temperatures. Despite the loss of the periodic ordering of the $FeCl_4^-$ ions in the amorphous phase of Bmim[$FeCl_4$], the existence of the oligomeric network of the $FeCl_4^-$ ions may be the origin of the antiferromagnetic interactions with low kinetic freedom at low temperatures.

We note that our present study ignored the conformers of MILs for the simplicity of the discussion. Although the anion-cation pair distribution functions are not significantly affected by the conformers in other ILs, the SDFs of the Fe around Emim or Bmim ions are sensitive to the conformation of the alkyl chains [25]. Further investigation of the detailed intermolecular structure of MILs will be necessary based on the results obtained from molecular dynamic simulations using flexible ion models; these studies will be carried out in the near future.

4. Conclusion

We have elucidated the magnetic IL structures of Emim[$FeCl_4$] and Bmim[$FeCl_4$] using HRMC simulations. The ERDFs for both MILs showed mutual cancelation of the anion-anion and anion-cation contributions that can give rise to misleading total ERDFs for both MIL structures, as shown in our HRMC analysis. The 1st coordination structure of the Emim and Bmim ions deduced from the SDFs was more distinct for Emim than that for Bmim, giving rise to their crystalline and amorphous states, respectively, at 90 K.

Finally, the studies of the temperature dependence of the Bmim[$FeCl_4$] structure showed a gradual structural change over a wide temperature range from 90 K to 523 K without a transition into a crystalline phase. In particular, distinct Cl$\cdots$Cl distances between the

neighboring $FeCl_4$ ions were observed at low temperature, indicating the pronounced antiferromagnetic interaction at low temperatures due to the freezing of the transitional and rotational motions in the amorphous Bmim[$FeCl_4$] structure.

Our structural investigation of MILs sheds new light on the development of MILs not only for practical applications but also for the advancing the basic science of pure liquids with a high magnetic response.

Acknowledgements

This research was supported by a Grant-in-Aid for Young Scientists (B) (No. 26870240), Young Scientists (A) (No. 17H04953) and Scientific Research (B) (17H03039). RF was partially supported by Takagi Research fund. The synchrotron radiation experiments were performed at the BL02B2 of SPring-8 with the approval of the Japan Synchrotron Radiation Research Institute (JASRI) (Proposal No. 2012B1438, No. 2013B1243, No. 2014A1167, and No. 2014B1196).

References

[1] M. Armand, F. Endres, D. R. MacFarlane, H. Ohno, B. Scrosati, Nature Materials, 8, (2009) 621-629.

[2] R. D. Rogers, K. R. Seddon, Science, 302 (2003) 792-793.

[3] M. Freemantle, An Introduction to Ionic Liquids, RSC Publishing, 2010.

[4] M. J. Earle, K. R. Seddon, Pure and Applied Chemistry, 72 (2000), 1391-1398.

[5] S. Hayashi, H. Hamaguchi, Chemistry Letters 33, (2004) 1590-1591.

[6] A. Joseph, G. Żyła, V. I. Thomas, P. R. Nair, A.S. Padmanabhan, S. Mathew, Journal of Molecular Liquids, 19, (2016) 319-331.

[7] A. García-Saiz, P. Migowski, O. Vallcorba, J. Junquera, J. A. Blanco, J. A. González, M.T. Fernández-Díaz, J. Rius, J. Dupont, J. R. Fernández, I. de Pedro, Chemistry - A European Journal, 20 (2014) 72-76.

[8] T. Inagaki, T. Mochida, Chemistry Letters, 39 (2010) 572-573.

[9] E. Santos, J. Albo, A. Irabien, RSC Advances, 4 (2014) 40008-40018.

[10] K. D. Clark, O. Nacham, J. A. Purslow, S. A. Pierson, J. L. Anderson, Analytica Chimica Acta, 934 (2016) 9-21.

[11] D. K. Bwambok, M. M. Thuo, M. B. J. Atkinson, K. A. Mirica, N. D. Shapiro, G. M. Whitesides, Analytical Chemistry, 85 (2013) 8442-8447.

[12] A. Mertelj, D. Lisjak, M. Drofenik, M. Čopič, Nature, 504 (2013) 237-241.

[13] I. de Pedro, D. P. Rojas, J. Albo, P. Luis, A. Irabien, J. A. Blanco, J. R. Fernández, Journal of Physics: Condensed Matter, 22 (2010) 296006.

[14] I. de Pedro, D. P. Rojas, J. A Blanco, J. R. Fernández, Journal of Magnetism and Magnetic Materials, 323 (2011) 1254-1257.

[15] T. Bäcker, O. Breunig, M. Valldor, K. Merz, V. Vasylyeva, A.-V. Mudring, Crystal Growth & Design, 11 (2011) 2564-2571.

[16] R. Hayes, G. G. Warr, R. Atkin, Chemical Reviews, 115 (2015) 6357-6426.

[17] S. H. Mir, L. A. Nagahara, T. Thundat, P. Mokarian-Tabari, H. Furukawa, A. Khosla, Journal of Electrochemical Society, 165 (2018), B3137-B3156.

[18] P. P. Shi, Q. Ye, Q. Li, H.-T. Wang, D.-W. Fu, Y. Zhang, R.-G. Xiong, Chemistry of Materials, 26 (2014) 6042-6049.

[19] A. H. Narten, M. D. Danford, H. A. Levy, Discussions of the Faraday Society, 43 (1967) 97-107.

[20] S. Bouazizi, S. Nasr, N. Jaîdane, M. C. Bellissent-Funel. The Journal of Physical Chemistry B, 110 (2006) 23515-23523.

[21] H. Katayanagi, S. Hayashi, H. Hamaguchi K. Nishikawa, Chemical Physics Letters, 392 (2004) 460-464.

[22] J. N. A. C. Lopes, A. A. H. Pádua, The Journal of Physical Chemistry B, 110 (2006) 3330-3335.

[23] S. Fukuda, M. Takeuchi, K. Fujii, R. Kanzaki, T. Takamuku, K. Chiba, H. Yamamoto, Y. Umebayashi, S. Ishiguro, Journal of Molecular Liquids, 143 (2008) 2-7.

[24] H. Morita, S. Kohara, T. Usuki. Journal of Molecular Liquids, 147 (2009) 182-185.

[25] K. Fujii, Y. Soejima, Y. Kyoshoin, S. Fukuda, R. Kanzaki, Y. Umebayashi, T. Yamaguchi, S. Ishiguro, T. Takamuku, The Journal of Physical Chemistry B, 112 (2008) 4329-4336.

[26] R. Futamura, T. Iiyama, Y. Takasaki, Y. Gogotsi, M. J. Biggs, M. Salanne, J. Ségalini, P. Simon, K. Kaneko, Nature Materials, 16 (2017) 1225-1231.

[27] S. K. Jain, R. J.-M. Pellenq, J. P. Pikunic, K. E. Gubbins, Langmuir 22 (2006) 9942-9948.

[28] T. Petersen, I. Yarovsky, I. Snook, D. G. McCulloch, G. Opletal, Carbon 41 (2003) 2403-2411.

[29] M. J. Frisch, G. Trucks, H. Schlegel, G. Scuseria, M. Robb, J. Cheeseman, G. Scalmani, V.Barone, B. Mennucci, G. Petersson, Gaussian 09, Revision A. 1, Gaussian, Inc., Walling-ford, CT, USA, 2009.

[30] C. M. Breneman, K. B. Wiberg, Journal of Computational Chemistry, 11 (1990) 361-373.

[31] R. Futamura, M. Jorge, J. R. B. Gomes, Theoretical Chemistry Accounts, 132 (2013) 1323-1324.

[32] S. Tsuzuki, A. A. Arai, K. Nishikawa, The Journal of Physical Chemistry B, 112 (2008) 7739–7747.

[33] T. Iiyama, K. Nishikawa, T. Suzuki, T. Otowa, M. Hijiriyama, Y. Nojima, K. Kaneko, The Journal of Physical Chemistry B, 101 (1997) 3037-3042.

[34] Y. Yoshida, G. Saito, Journal of Materials Chemistry, 16 (2006) 1254-1262.

[35] M. Yoshimoto, R. Futamura, A. Hoshikawa, T. Ishigaki, T. Uchida, T. Iiyama, Chemistry Letters, 46 (2017) 923-925.

[36] A. García-Saiz, I. de Pedro, J. A. Blanco, J. González, J. R. Fernández, The Journal of Physical Chemistry B, 117 (2013) 3198-3206.

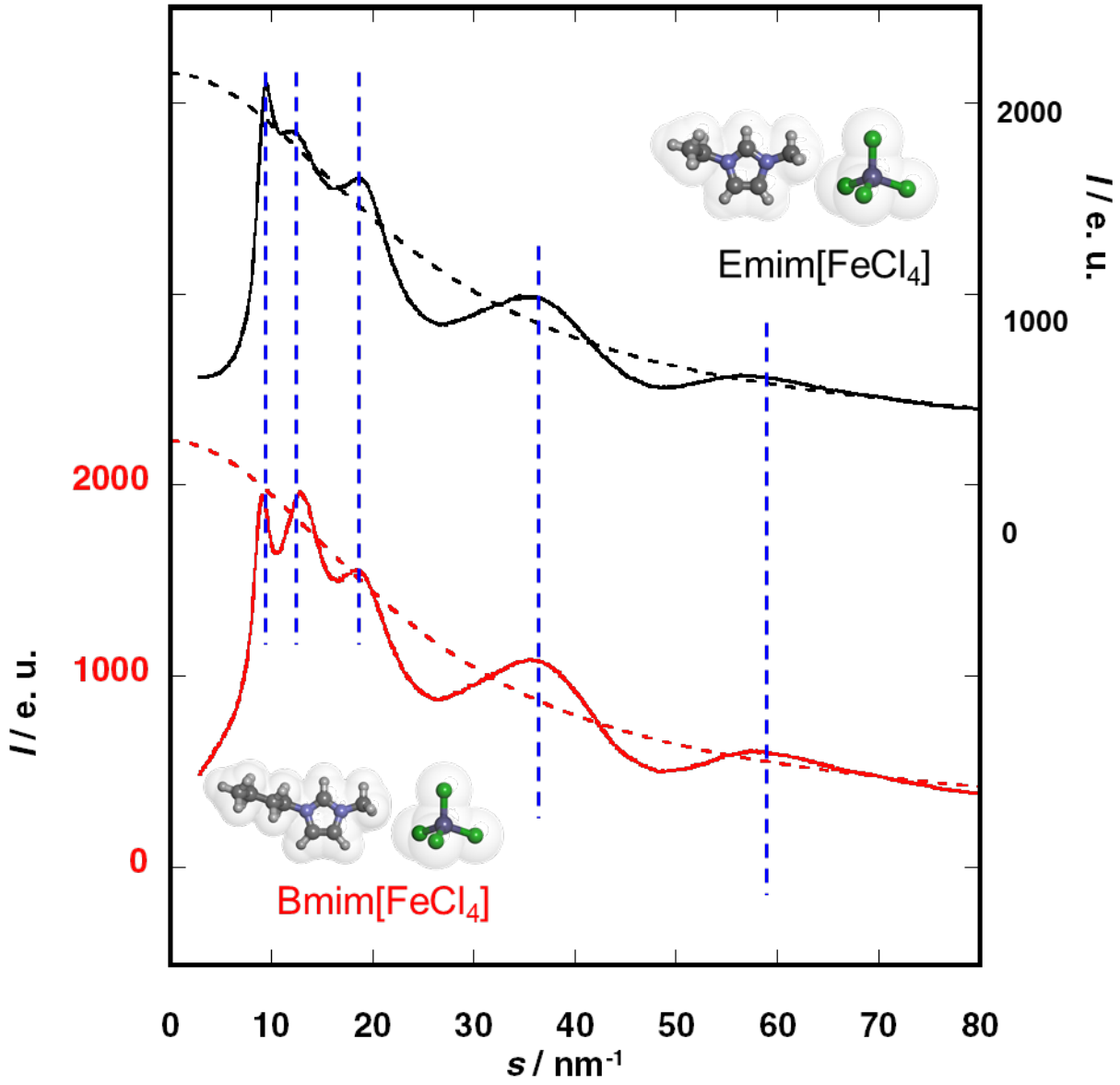

Fig. 1. Corrected X-ray scattering profiles of Emim[$FeCl_4$] (top) and Bmim[$FeCl_4$] (bottom). The dashed curves indicate the sum of the independent atomic scattering profiles of each IL. Vertical blue dashed lines indicate the peak positions of Emim[$FeCl_4$] provided to guide the eye.

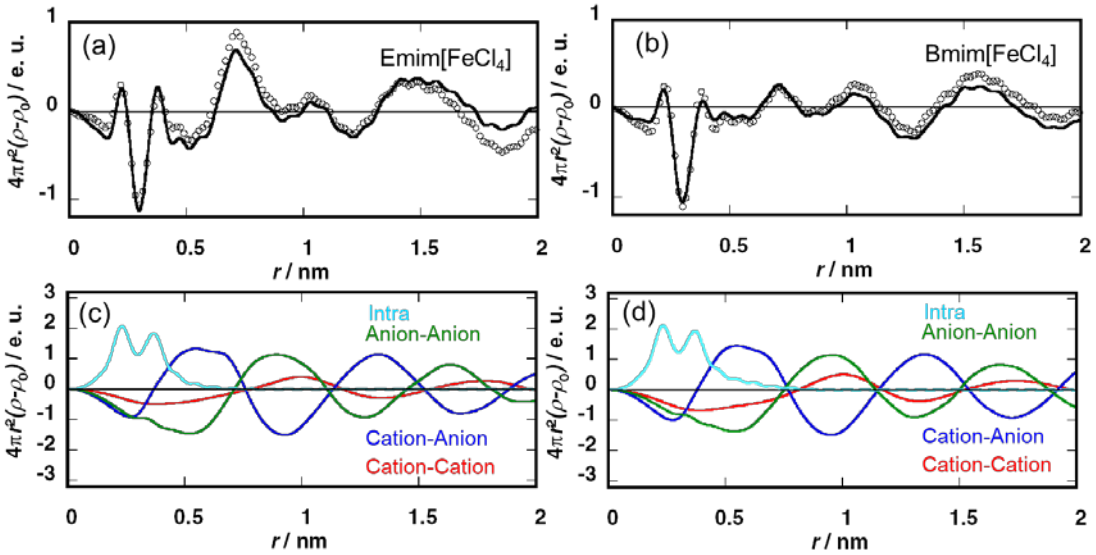

Fig. 2. (a,b) Electron radial functions (ERDFs) of (a) Emim[$FeCl_4$] and (a) Bmim[$FeCl_4$]. Open circles and solid lines denote the experimental results and the results of the HRMC simulations, respectively. (c,d) Each component ERDF obtained by HRMC simulations for (c) Emim[$FeCl_4$] and (d) Bmim[$FeCl_4$], with intra-molecule (sky blue), inter anion (green), inter cation-anion (blue), and inter cation (red) components shown.

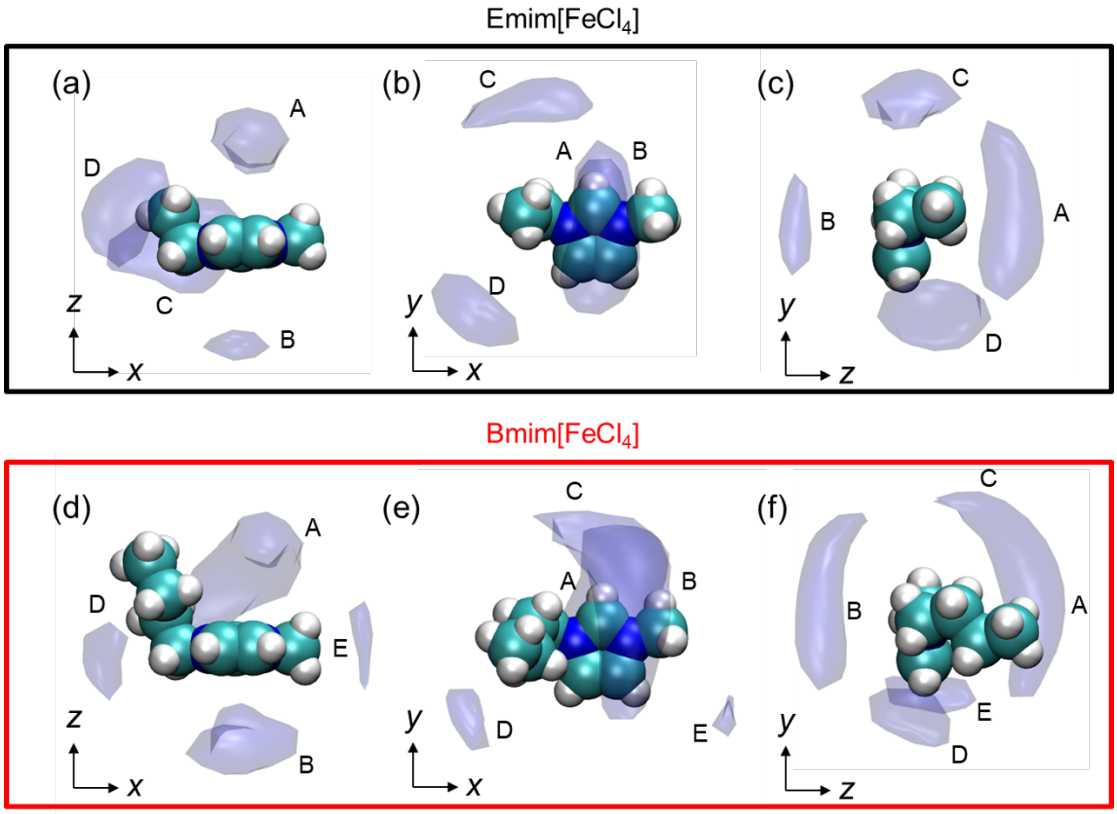

Fig. 3. Spatial distribution functions (SDFs) of Emim[$FeCl_4$] (top) and Bmim[$FeCl_4$] (bottom) for the 1st coordination structure of Fe around the cations evaluated by HRMC simulations. In these figures, the plane of the imidazolium ring is parallel to the *x*-*y* plane and the *z* direction is perpendicular to the *x*-*y* plane. Cyan, blue, and white spheres represent carbon, nitrogen, and hydrogen atoms, respectively.

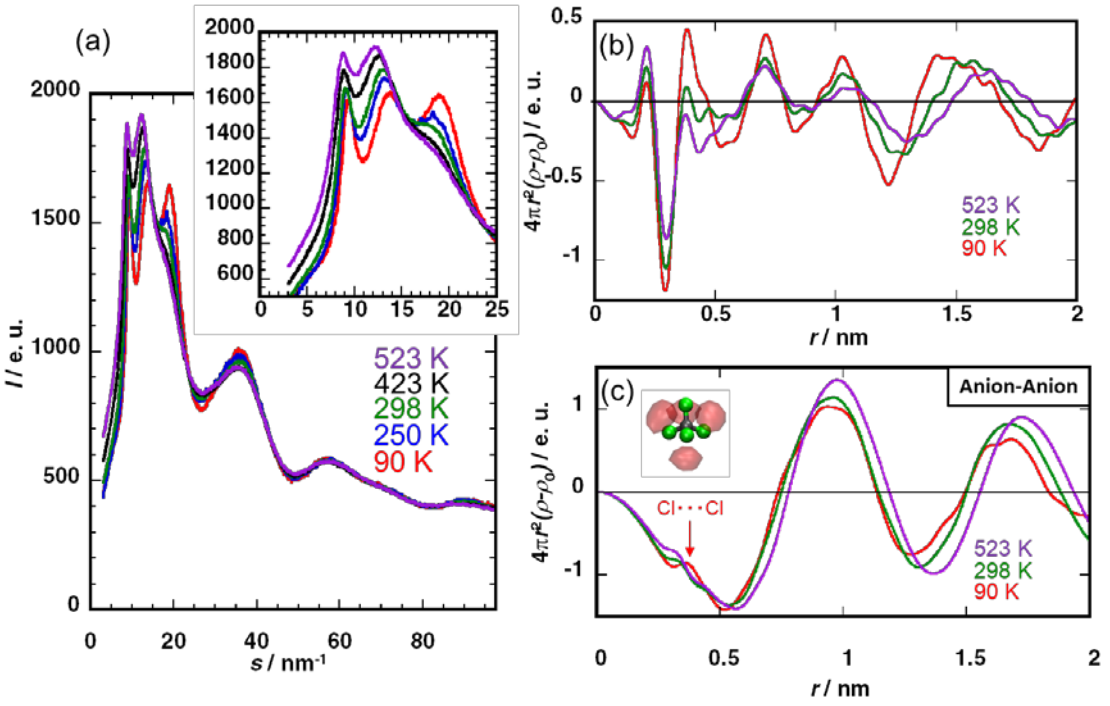

Fig. 4. (a) Temperature dependence of the X-ray scattering profiles of Bmim[$FeCl_4$] from 90 K to 523 K. (b) ERDFs of Bmim[$FeCl_4$] at 90 K (red), 298 K (green), and 523 K (purple). (c) Component anion-anion ERDFs evaluated by HRMC simulations for Bmim[$FeCl_4$] at 90 K (red), 298 K (green), and 523 K (purple). Inset shows the SDF of the nearest Cl atoms around the $FeCl_4$ ion at 90 K. Here, green and gray spheres represent the chlorine and iron atoms of the $FeCl_4$ ion, respectively.

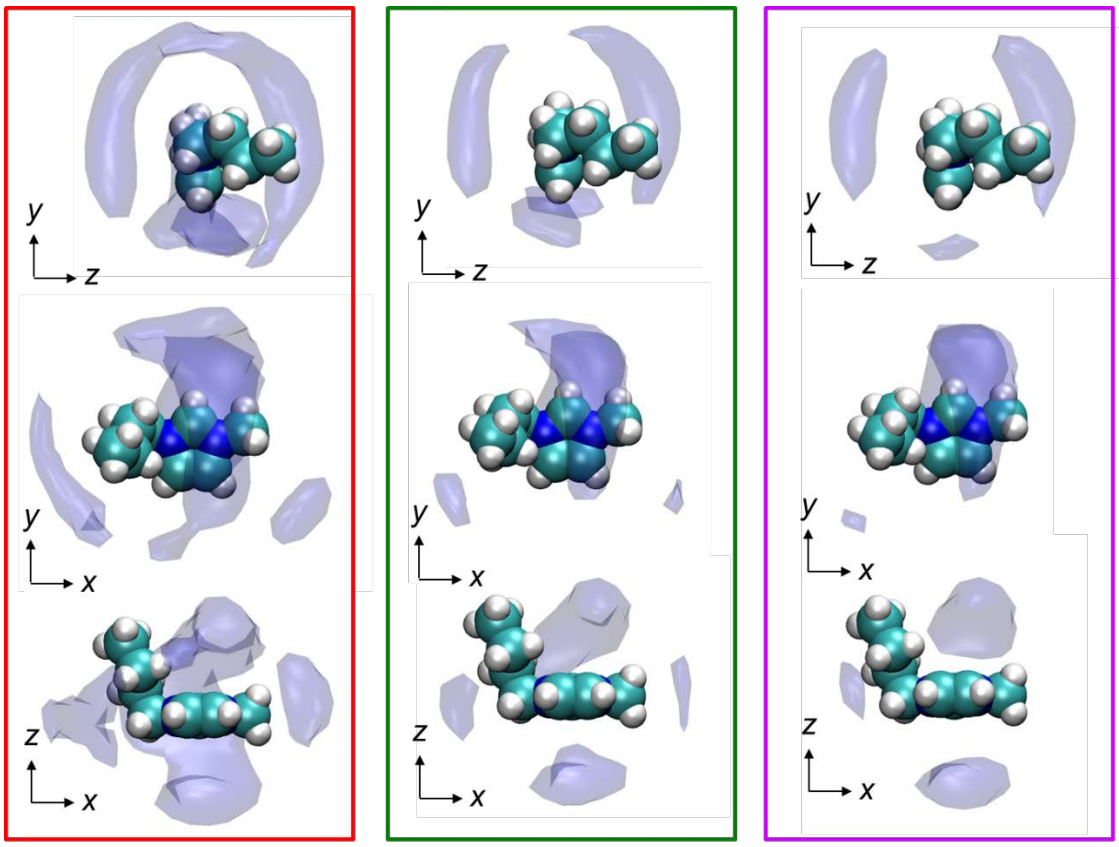

Fig. 5. Spatial distribution functions of Bmim[$FeCl_4$] for the 1st coordination structure of Fe around the cations evaluated using HRMC simulations at 90 K (left), 298 K (center), and 523 K (right). In these figures, the plane of the imidazolium ring is parallel to the *x*-*y* plane, and the *z* direction is perpendicular to the *x*-*y* plane.

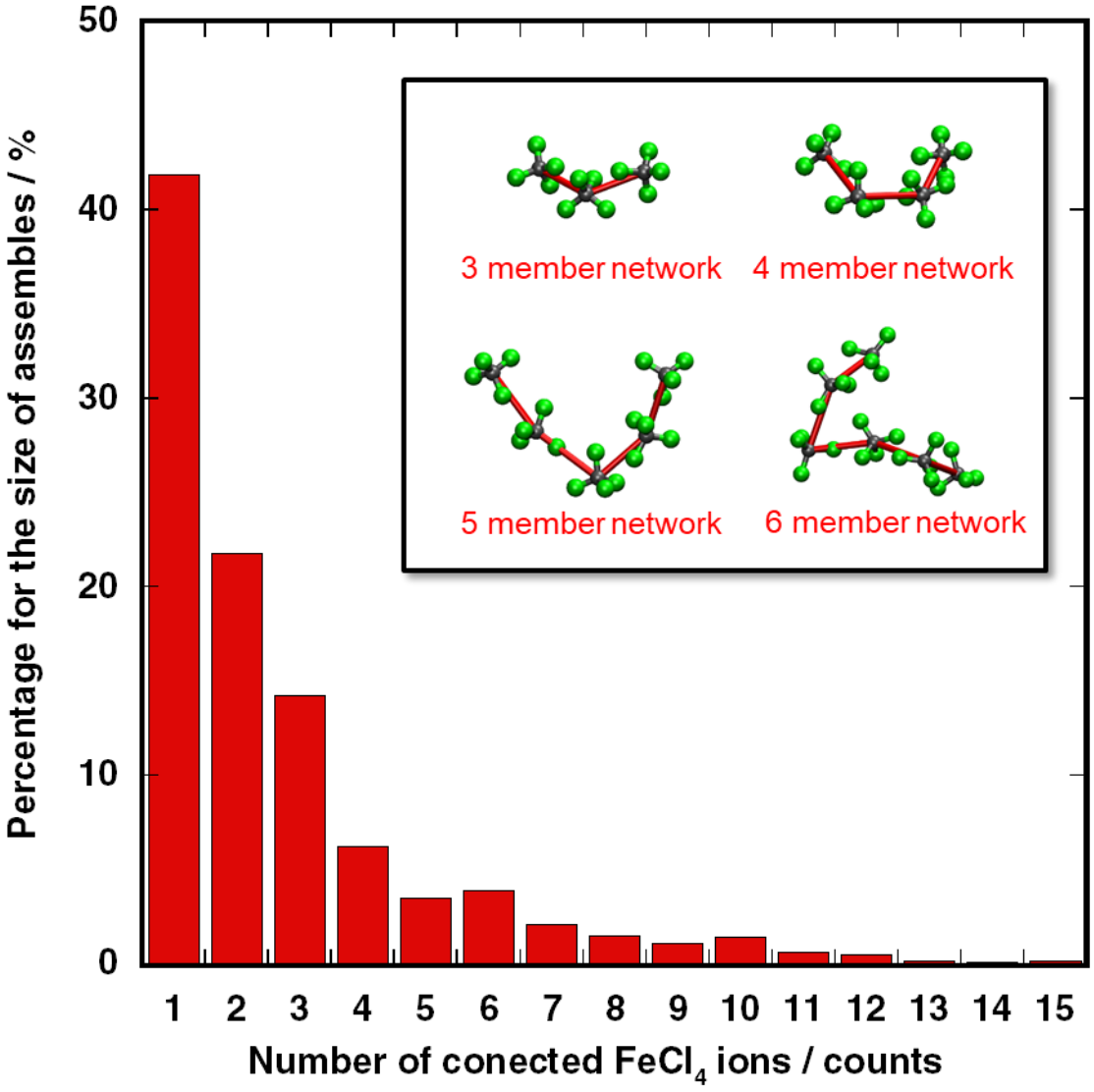

Fig. 6. Distribution of the assembling number of neighboring $FeCl_4^-$ ions in Bmim[$FeCl_4$] at 90 K. Here, we defined the Cl-Cl neighbor distance as less than 0.39 nm. (Inset) 3-, 4-, 5-, and 6-member networks of $FeCl_4^-$ ions in the simulation snapshot. Green and gray spheres represent the Cl and Fe atoms, respectively. Red lines connect the Fe atoms in the Fe-Cl-Cl-Fe networks.